HHS Public Access

Author manuscript

ACS Nano. Author manuscript; available in PMC 2022 October 26.

Published in final edited form as:

ACS Nano. 2021 October 26; 15(10): 16697–16708. doi:10.1021/acsnano.1c06672.

Universal polymeric-to-colloidal transition in melts of hairy nanoparticles

Daniele Parisi[1], **Eileen Buenning**[2], **Nikolaos Kalafatakis**[1], **Leo Gury**[1,3], **Brian C. Benicewicz**[4], **Mario Gauthier**[5], **Michel Cloitre**[3], **Michael Rubinstein**[6,7], **Sanat K. Kumar**[2], **Dimitris Vlassopoulos**[1]

[1]University of Crete, Department of Materials Science and Technology, and FORTH, Institute of Electronic Structure and Laser, Heraklion, Greece.

[2]Department of Chemical Engineering, Columbia University, New York, NY 10025, USA.

[3]Molecular, Macromolecular Chemistry and Materials, ESPCI Paris, CNRS, PSL Research University, 75005 Paris, France

[4]Department of Chemistry and Biochemistry, University of South Carolina, Columbia, SC 29208, USA

[5]Department of Chemistry, Institute for Polymer Research, University of Waterloo, Waterloo, Ontario, Canada N2L 3G1

[6]Departments of Mechanical Engineering and Materials Science, Biomedical Engineering, Chemistry, and Physics, Duke University, Durham, NC 27708, USA

[7]Institute for Chemical Reaction Design and Discovery (WPI-ICReDD), Hokkaido University, Sapporo 001-0021, Japan

Abstract

Two different classes of hairy self-suspended nanoparticles in the melt state, polymer-grafted nanoparticles (GNPs) and star polymers, are shown to display universal dynamic behavior across a broad range of parameter space. Linear viscoelastic measurements on well-characterized silica-poly(methyl acrylate) GNPs at fixed core radius (R_{core}) and grafting density (or number of arms f), but varying arm degree of polymerization (N_{arm}) show two distinctly different regimes of response. A colloidal Regime I at small N_{arm} (large core volume fraction), with a predominant low-frequency solid-like colloidal plateau and ultraslow relaxation, and a polymeric Regime II at large N_{arm} (small core volume fractions), with a response dominated by the star-like relaxation of partially interpenetrated arms. The transition between the two regimes is marked by a cross-over where both polymeric and colloidal modes are discerned albeit without a distinct colloidal plateau. Similarly, polybutadiene multiarm stars also exhibit the colloidal response of Regime I at very large f and small N_{arm}. The star arm relaxation model and a simple scaling model of nanoparticle escape from the cage of neighbors by overcoming a hopping potential barrier due to their elastic

Supporting Information

Conceptualization of topological jamming; Linear viscoelastic measurements and analysis; A simple brush conformation model; Modeling of polymeric arm relaxation; Slow mode analysis; Linear viscoelastic master curves of multiarm star polymer melts; X-ray scattering analysis.

deformation, describe quantitatively the linear response of the polymeric and colloidal regimes, respectively, in all these cases. The dynamic behavior of hairy nanoparticles of different chemistry and molecular characteristics, investigated here and reported in the literature, can be mapped onto a universal dynamic diagram of $\frac{f}{\left(R_{core}^3/v_0\right)^{1/4}}$ as a function of $\frac{N_{arm}v_0 f}{R_{core}^3}$, where v_0 is the monomeric volume. In this diagram, the two regimes are separated by a line where the hopping potential ΔU_{hop} is equal to the thermal energy, k_BT. ΔU_{hop} can be expressed as a function of the overcrowding parameter x, i.e. the ratio of f to the maximum number of unperturbed chains with N_{arm} that can fill the volume occupied by the polymeric corona, hence this crossing is shown to occur when x=1. For x>1 we have colloidal Regime I with overcrowded volume, stretched arms and $\Delta U_{hop} > k_BT$, while polymeric Regime II is linked to x<1. This single material parameter x can provide the needed design principle to tailor the dynamics of this class of soft materials across a wide range of applications from membranes for gas separation to energy storage.

INTRODUCTION

Grafting polymer chains onto a nanoparticle is a typical strategy to promote miscibility and homogeneity in nanocomposites.[1–5] Grafted nanoparticles (GNP) comprise a hard inorganic (hydrophilic) core and an organic (polymeric) shell; their surfactant-like structure makes them attractive as hybrid building blocks for hierarchical assemblies and new functional materials.[6] The presence of grafted chains prevents nanoparticle aggregation, although this strongly depends on the surface coverage. Interparticle interactions can be strongly affected and tuned by changing the degree of polymerization of the tethered chains, the grafting density, the grafting density distribution and the size of the core. Most often, GNPs are dispersed in a matrix of polymer chains or oligomers having the same chemistry as the grafted chains. Several theoretical, experimental and computational approaches have been used in the last 30 years to investigate the structural properties and dynamics of these systems.[3–14]

When GNPs or star polymers (which represent the limiting case of GNPs with a very small core) or ordered block copolymer spherical micelles are self-suspended in the melt state, i.e., in solvent-free conditions, they interact in a completely different way in comparison to the case in which they are placed in a polymeric matrix or a molecular solvent.[3,15–28] This is the focus of the current work. In fact, GNPs with high enough grafting density and long enough grafted chains are well-dispersed and interact primarily via their coronas which can interpenetrate.[14] It was shown[4] that such suspensions exhibit multiscale structural transitions (e.g., the GNPs organize into crystalline lattices) and improved conformational stability as a result of strong steric repulsion between the grafted chains and space-filling constraints on the tethered chains in the single-component self-suspended material. Recently, it has also been shown that self-suspended GNPs are characterized by slow equilibration dynamics and structural evolution with time.[29] In fact, Archer *et al.*[29] determined, by using a combination of rheological and X-ray scattering measurements, that neat GNPs exhibit structural peaks which become enhanced over time, as a consequence of the significant equilibration process involving local rearrangements of the grafted chains. This feature was shown to be accompanied by an increase of the strength of the effective cage (which reflects

the topological constraints of neighboring particles), as evidenced by the time evolution of the plateau storage modulus. Another study[20] reported the absence of terminal flow within the experimentally accessible time window. Such behavior was attributed to the coupling between arm interpenetration and particle localization (due to interparticle interactions); however, there was no explicit discussion of structural or jamming dynamics, i.e., the decoupling of polymeric and colloidal modes.

In this context, it is instructive to consider multiarm star polymer melts, which represent an important class of model self-suspended grafted nanoparticles (with zero core radius) which have been investigated extensively.[30–32] In particular, it was shown that melts of stars with a functionality f=64 or 128, and number of entanglements per arm between 4 and 43 exhibit a two-step stress relaxation, comprising a polymeric arm relaxation and a slow colloidal mode.[13,33] The latter was associated with the liquid-like ordering of the stars and attributed to a cooperative hopping process akin to cage escape in colloidal glasses.[33] Recently, experimental results with stars of very high functionality (f>850) and low arm size (2–3 entanglements) indicate a substantial dynamic arrest with dramatic slowing-down of the topologically constrained colloidal mode, which was assigned to colloidal jamming.[34] These findings call for a deeper understanding of the colloidal jamming transition in melts of hairy nanoparticles and question its potential universality with a final ambitious goal to obtain the needed ingredients to describe jamming from hard spheres (point contacts, see also Figure S1 of the SI) to deformable impenetrable spheres (facets) to hairy spheres and to star polymers (interpenetration).

Recent simulations[8] have shown that the structural relaxation of self-suspended GNPs with long chains have higher relative diffusivities than their short chain counterparts, which may exhibit caging analogous to that of hard spheres. Depending on the GNP's internal microstructure, i.e., the number and size of grafted chains, the segments of the grafted chains near the particle surface can be stretched or effectively frozen. A point of crucial importance is the degree to which the coronas of densely grafted particles can interpenetrate. Theoretical analysis of polymer brushes in contact with chemically identical homopolymers shows that low molar mass homopolymers (free melt chains penetrate and swell the brush), whereas for high molar mass homopolymers this interpenetration and swelling occurs only partly.[35–37] For pure GNP melts with the same grafting density, increasing the size of the grafts should initially reduce the relative amount of interpenetration due to enhanced stretching of the inner section near the core.[33,35,36] However, further increases in the graft size would saturate the inner chain stretching and increase the interpenetration like in star polymers. Recent coarse-grained molecular dynamics simulations on GNP melts[38] demonstrated that the chain extension free energy is nonmonotonic as the molar mass of the grafted chains increases at a fixed grafting density. A maximum in free energy was detected, corresponding to the crossover from a dry layer-dominated to an interpenetration layer-dominated brush conformation regime.[38]

In the past few years, GNPs were proposed as promising candidates for gas separation membranes.[39–43] Membranes of self-suspended poly(methyl acrylate)-grafted silica nanoparticles exhibited elevated gas permeability with respect to the corresponding linear polymer chains.[43] The effectiveness of these membranes depended on the molar mass of

the tethered chains in a non-monotonic way. This was linked to an increase in effective free volume, which was defined as the unoccupied (interstitial) volume, which in turn depended on the grafting density and the graft molar mass.[15,44] These interesting developments and related technological challenges necessitate the ability to tailor the properties of GNPs. Hence, they pose a fundamental question: how do the dynamics of self-suspended GNPs depend on their internal microstructure?

In the present work, we address the above challenge using a series of poly(methyl acrylate)-grafted silica nanoparticles (PMA- SiO_2), which essentially have a fixed grafting density but different degrees of polymerization (see Table M1) and multiarm polybutadiene stars of very high functionality and relatively small arm degree of polymerization (see Table M2). It was shown in previous investigations[15,30] that such model nanoparticles with a uniform grafting density are homogeneously distributed into a spatially amorphous structure. We quantitatively describe the polymeric and colloidal contributions to the dynamics of these soft colloids. We identify the threshold marking the transition from polymeric-dominated to colloidal-dominated response, and propose a generic dynamic diagram, where data from star polymers and GNPs are unified into a plot with regimes corresponding to different behaviors.

RESULTS AND DISCUSSION

Linear viscoelastic properties.

Master curves of the storage moduli, loss factors, and shift factors for GNP samples 196k, 94k and 33k (we use for simplicity this nomenclature, see Table M1) are shown in panels A, B and C of Figure 1, respectively (full spectra are provided in Figure S2 in the SI). The master curves of the storage moduli G' (Figure 1A), are obtained from the time temperature superposition principle (tTS) (see Figure S3 of the SI for the validity of the tTS) and creep conversion (see Figures S4–S7); they cover nearly 16 decades in frequency, from the glassy regime to the structural relaxation of the system. The master curves are shown at the same temperature distance (40 °C) from the glass transition temperature (T_g), as an increase in silica content resulted in a slight T_g increase (see Table M1 and Figure S2 of the SI). Under these conditions, monomeric iso-friction conditions are guaranteed for comparison among particles with different degrees of polymerization (or silica contents). Moreover, we note that the combination of high grafting densities and topology, which is responsible for the “dry” and “wet” layer conformations of GNPs and stars, gives rise to regimes of distinct local mobility.[45–47] In the present work we focus on large-scale dynamics associated with the response of grafted arms and of the entire nanoparticle. The results indicate rich relaxation dynamics with both polymeric and colloidal contributions observable in the same rheological spectrum and occurring at different time (and length) scales. These spectra show qualitative resemblance with recent results obtained for star polymers of very high functionality.[34] With decreasing frequency, all the specimens show a glassy regime (in high-frequency region for $\omega a_T > 10^5$ rad/s in Figure 1A) followed by a transition region and a polymeric plateau associated with arm entanglements. The latter is consistent with the behavior of pure PMA chains (about 0.25 MPa).[48] However, an increase in the plateau value is detected as the silica content in the samples increases (or the degree

of polymerization of the tethered chains decreases). This filler reinforcement effect follows a Guth-Gold[49,50] trend with the silica volume fraction (see Figure S8 of the SI). The chain entanglement plateau extends on the frequency scale as the degree of polymerization of the grafted chains increases (see Figure 1A). This is reminiscent of the arm retraction relaxation mechanism[51] reported in several experimental studies on star polymers.[33,52] Indeed, if one imagines grafting significantly longer chains, so that the core becomes relatively small in size as compared with the polymer chains, the star-polymer limit should be reached, which is apparently the case for the 196k sample (green line), i.e., the linear viscoelastic modulus decreases with decreasing frequency until the terminal regime is reached, as expected.[52]

A more interesting behavior is observed when the grafted chains are shorter. Indeed, for $M_{arm} \leq 94$ kg/mol (with about 8.5 entanglements) we see an unambiguous additional mode characterized by a low-frequency plateau, which is about 100 times lower in comparison to the entanglement plateau, and an eventual relaxation which is about 1000 times slower than for the 196k sample. Despite the eventual terminal relaxation, we attribute this unusually slow time and low plateau modulus to a jammed colloidal material (i.e., with predominant solid-like character),[29,34] as discussed further below. It should be noted that soft colloidal glasses with an observable alpha relaxation have been discussed in the literature.[16–18,53,54] These findings suggest that upon reducing the arm molar mass, the polymer-dominated response is augmented by a hierarchical relaxation mechanism where arm retraction is followed by a colloidal relaxation process. Colloidal cage-escape[55,56] dynamics continue until structural relaxation of the system takes place, as proposed for multiarm star polymers.[33,34] It is important to note that the lowest four frequency decades are not accessible by means of the tTS, as the temperatures required to reach these frequencies in conventional small-amplitude oscillatory shear measurements are prohibitively high and the samples would degrade. To overcome this issue, creep experiments were performed and the measured compliances were converted into dynamic moduli (see Figures S4–S7 of the SI).[57–59]

Rheological spectra can also be analyzed using the loss factor ($\tan\delta = G''/G'$) as a function of frequency (Figure 1B). This representation facilitates the determination of the characteristic times of the materials, as the inverse frequency at the loss factor peaks or the moduli crossover ($\tan\delta=1$), as indicated by arrows in Figure 1B.[60,61] From high to low frequencies the following characteristic reciprocal frequencies (identifying relaxation times) are depicted in Figure 1B: the segmental relaxation time of a Kuhn monomer τ_0, the Rouse relaxation time of an entanglement strand τ_e, the arm retraction time τ_{arm} and the structural or terminal relaxation time τ_{term}. Note that τ_0 and τ_{arm} refer to relative maxima in $\tan\delta$, which imply maximum viscous dissipation in the system, while τ_e and τ_{term} are estimated as the inverse frequency at which $\tan\delta = 1$.[51,61] Whereas there is a clear distinction between τ_{arm} and τ_{term} for samples 94k and 33k, only one characteristic time, τ_{term}, is clearly observed for sample 196k (with about 18 entanglements), as the colloidal regime disappears and arm relaxation apparently becomes the terminal relaxation process. Moreover, τ_e and τ_0 are independent of the degree of polymerization of the chains (provided that the polymers are at least one entanglement long) and coincide for all the systems (see Table S1 of the SI). The frequency dependence of the loss factor can also serve to obtain the polymeric

intermediate-frequency plateau modulus, $G_{plateau}$, and the colloidal low-frequency plateau modulus associated with entanglements, G_{LF}, as discussed below. These quantities coincide with the storage modulus at the angular frequency where the loss factor exhibits a relative minimum, in other words, where the elasticity of the system is the highest (see the arrows in Figure 1B). The characteristic times and plateau moduli are reported in Table S1 of the SI. Note also that for all the GNP melts studied we found uniform spatial organization of densely packed objects whose center-to-center distance scales with the total molar mass with a power-law exponent of 1/3 (see Figures S26–27 and X-ray scattering analysis section of the SI).

Horizontal (a_T) and vertical (b_T) shift factors are reported in Figure 1C along with those for pure PMA linear chains. The a_T values for the GNPs do not differ from the pure PMA chains and their temperature dependence is well-described by the Williams-Landel-Ferry (WLF) empirical equation[62] with constants C_1 = 6.9 and C_2 = 93.2 K at T_{ref} = 60 °C (neat PMA). This highlights an important finding, that despite of the existence of the colloidal mode, the dynamics are still controlled by the monomeric friction dependence on temperature. This may not be the case for lower grafting densities but this challenge goes beyond the scope of this work. The vertical shift factors b_T only depend on the temperature variation of the PMA density and can be described by a polynomial function of the absolute temperature, as reported in the literature.[63] The density varies by less than about 20% over the range of temperatures investigated. One may argue that the experimental samples contain a large fraction of silica, hence, this should be also taken into account for the density variation. However, significant density variations for silica are only expected above 2000 K,[64] well above the temperature range probed in our experiments.

Simple model for the dynamics of jammed GNPs.

The main finding of this work is that the GNP melts undergo a viscoelastic liquid-to-jamming transition for grafted arm molar masses between 94k and 196k. It is important to emphasize that the experimental signatures of jamming are the presence of a low-frequency plateau modulus and an extremely slow or inaccessible terminal relaxation. To better understand this transition, as well as the tendency for the largest grafted arm 196k sample to behave akin to a star polymer melt, we examined separately the polymeric and colloidal contributions to stress relaxation. To this end, we followed a synergistic three-step approach consisting of (i) the analysis of arm relaxation through tube modeling (for entangled arms), (ii) consideration of the structure of the grafted polymer layer with a region close to core where chains of neighboring particles cannot penetrate (dry layer), and an outer region where chain interdigitation occurs (wet layer), and (iii) analysis of the colloidal cage escape mode by invoking a hopping potential of the elastically deformed jammed particles.

First, we analyzed the polymeric response using the Milner-McLeish (MM) tube model for stars[33,65] accounting also for fast Rouse and longitudinal modes.[66,67] We identified the experimental polymeric relaxation time (Figure 1B, Table S1), and determined the fraction of the grafted arm s_{eff} that relaxes according to the MM model (i.e., the degree of interpenetration), by fitting the theoretical stress relaxation modulus $G(t)$ (which is a function of the size of the disentangling sections of arms) up to a characteristic size that

corresponds to the experimental polymeric time. Even though this time represents only the relaxation of a fraction of the arm (s_{eff}), we call it τ_{arm} hereafter. The relaxation modulus $G(t)$ as per Milner-McLeish is given by

$$G(t) = G_{plateau}\left\{\frac{1}{Z}\sum_{p=Z}^{N_{arm}} exp\left(-\frac{2p^2t}{\tau_R}\right) + \frac{1}{5Z}\sum_{p=1}^{Z-1} exp\left(-\frac{2p^2t}{\tau_R}\right) + (x+1)\int_0^{s_eff}(1-s)^x exp\left[\frac{-t}{\tau_{arm}(s)}\right]ds\right\} \quad (1)$$

where the first two terms in the right-hand side of eq.1 represent the fast Rouse and the longitudinal modes, respectively, with τ_R being the Rouse time of the arm, estimated as $\tau_R=\tau_e Z^2$, and τ_e is the relaxation time of an entanglement strand containing N_e monomers, and $Z=N_{arm}/N_e$ is the number of entanglement strands per chain. The quantity $x = 4/3$ is the dilution exponent,[51,65,68] and $\tau_{arm}(s)$ is the arm relaxation time involving the early sub-diffusive and the late activated modes, as described by the MM model.[33,65] The upper limit of the integral s_{eff} is determined from the fit to the experimental data and provides a decent approximation of the fraction of the arm that has relaxed via arm retraction. This scenario is illustrated in the idealized schematic shown in Figure 2. The grafted chain can be divided into two sections: (i) an inner "dry" layer which is close to the nanoparticle core and is not interpenetrated by the chains of neighboring nanoparticles, and (ii) an outer layer, which is interpenetrated by chains from other GNPs and is called "interpenetrated or wet layer".[34–36,38] The former comprises a fraction ($1\text{-}s_{eff}$) of the grafted chain which we propose, as a first approximation, to be associated with an average molar mass $M_{1\text{-}seff} = (1\text{-}s_{eff})\ M_{arm}$, and the latter corresponds to a chain fraction s_{eff} with a respective molar mass $M_{seff} = s_{eff}\ M_{arm}$. We emphasize that, while in our analysis we used the average molar mass of the interpenetrating arm, however, in reality, there is a distribution in each layer that may lead to a broader spectrum of arm retraction times; this has been treated rigorously in the literature.[33,69] We also ignored the fact that not all the arms are expected to enter the interpenetration zone. Depending on their internal microstructure (which is controlled by f and N_{arm}), there are GNPs exhibiting predominantly a jammed colloidal response (Regime I in Figure 2) and GNPs with a polymeric response (Regime II in Figure 2). It should be noted that application of the MM tube model to highly grafted brushes with a low M_{arm}, $Z < 5$, is not rigorous,[34] and hence we mainly restrict our discussion to brushes with $Z > 5$. The transition from the "predominantly colloidal" Regime I, where the GNP melts exhibit jammed colloidal response akin to caged particles,[34] to "predominantly polymeric" Regime II, where relaxation of the mutually interpenetrated grafted arms controls the GNP response, is not sharp. Instead, there is an intermediate situation without clear colloidal plateau, with arm retraction and colloidal relaxation modes close to each other, albeit distinct, corresponding to a colloidal hopping potential (discussed below) exceeding thermal energy and well-entangled arms (see Figures 8 and S2, S16, and S17 of the SI).

Typical MM fitting results (eq. 1) are presented in Figure 3 for two cases: a polymeric-arm dominated Regime II (for the highest arm molar mass studied, 196k) and a situation where both polymeric and colloidal responses are clearly discerned (for M_{arm}=94kg/mol). This

figure depicts the dynamic moduli, after converting the stress relaxation modulus of eq. 1,[60] and the resulting effective degree of polymerization of the interpenetrated sections of arms (s_{eff}) determined from these fits is listed in the legend. The fits to the MM model for the other arm molar masses are reported in Figures S15–S20 of the SI. GNPs with long arms, i.e., M_{arm} > 94 kg/mol, are not jammed (the potential barrier for colloidal hopping discussed below is lower than k_BT and Z>>1) and relax similarly to star polymers (Regime II in Figure 2), while GNPs with shorter arms ($M_{arm} \leq$ 94 kg/mol) exhibit a response akin to soft colloidal jamming (Regime I in Figure 2). The results of the MM fits in terms of arm relaxation time and interpenetrated Kuhn degree of polymerization (corresponding to fraction s_{eff}, of the grafted arm in Figure 2) are reported in Table S3 of the SI. A more rigorous determination of the degree of polymerization of the interpenetrated layer, N_{inter}, is based on the use of a brush conformation model and is presented in the SI (Figures S12 and S13A). Once the average N_{inter} in each layer is known, the respective thickness can be estimated from the brush conformation model (Figure S13B). In this context, the fraction of dry (non-interpenetrated arm) material, expressed as the ratio M_{dry}/M_{arm}, was also determined and is displayed in Figure S14. This quantity is inherent in the overcrowding parameter, x, which is the ratio of number of grafted arms f to the maximum number of unperturbed chains with N_{arm} that can fill the volume occupied by the polymeric corona (see SI and Ref. 38). We show below that this single parameter determines the predominantly polymer or colloidal response in the GNPs and other hairy nanoparticles.

We now analyze the slow colloidal response of the GNPs and in particular those belonging to the jamming Regime I. In this case, after relaxation of their arms, the GNPs remain jammed, i.e., trapped into effective cages and attempt to escape them by hopping. To undergo hopping between neighboring cages, a GNP needs to overcome a free energy barrier ΔU_{hop}.[33,34,70–72] The cage escape process is characterized by a terminal relaxation time

$$\tau_{term} \approx \tau_{attempt} exp\left[\frac{\Delta U_{hop}}{k_BT}\right] \quad (2)$$

where the attempt time $\tau_{attempt}$ is estimated following the analysis of Kapnistos *et al.*[33] We suggest that the cage escape of GNPs with respect to their neighbors requires disengagement/re-engagement of the arms and hopping. The friction coefficient of a GNP is proportional to the number of arms, f = 378 times the effective friction per arm ~ $k_BT\tau_{arm}/(\Delta R)^2$. We estimated the displacement of the interpenetrated section of an arm during retraction (over the time scale τ_{arm}) by the thickness of the interpenetrated zone (red section in Fig. 2), $\Delta R \approx bN_{inter}^{1/2}$, considered to be Gaussian,[33,38] with b= 1.47 nm being the Kuhn monomer length.[48] The corresponding displacement of the entire GNP due to single arm retraction is $\frac{\Delta R}{f}$. The mean square displacement for such a single event is $\frac{(\Delta R)^2}{f^2}$, while there are f such events during the time interval τ_{arm}. This yields an "attempt" diffusion coefficient for the GNP within a cage:

$$D_{attempt} \approx f\frac{(\Delta R)^2}{\tau_{arm} f^2} \quad (3)$$

The hopping step has a very low probability in this crowded environment, and hence many attempts are needed for a jammed GNP to escape from its effective cage. The respective attempt time is on the order of the diffusion time of the GNP over a distance comparable to its total radius R in the absence of potential barrier, where the total radius of the GNP is

$$R = \left[\left(R_{core}^3 + \frac{3}{4\pi}\upsilon_0 f N_{arm}\right)\right]^{1/3} \quad (4)$$

R_{core} = 8 nm is the average (volume averaged) radius of the silica core, N_{arm} is the Kuhn degree of polymerization of the graft with a molar mass M_{arm}, $\upsilon_0 = \frac{M_0}{N_A \rho}$ is the volume of the Kuhn monomer (υ_0 = 0.673 nm^3 for a Kuhn molar mass M_0 = 494.6 g/mol[48] and ρ = 1.22 g/cm^3 [63]). The total particle radius calculated from eq. 4 is in good agreement with the characteristic length extracted from X-ray measurements (see Figures S26 and S27 of the SI).

The attempt time is therefore proportional to the square of the diffusion distance R^2 divided by the attempt diffusion coefficient $D_{attempt}$ (eq. 3), which yields:

$$\tau_{\text{attempt}} \sim \frac{R^2}{D_{attempt}} = a\tau_{\text{arm}} f \frac{R^2}{(\Delta R)^2} \quad (5)$$

where a is a coefficient determined from the best fit of the experimental terminal relaxation times as discussed below; it is found to be equal to 2. The arm relaxation time τ_{arm} in eq. 5 can be estimated either by using the experimental value (Figure 1 and Table S1) or with the MM model, using N_{inter} extracted from the two-layer brush conformation model (see Table S4 of the SI and Figure 8 below).[38] The GNPs with the largest M_{arm} > 130 kg/mol are excluded from this analysis, as in the absence of a colloidal barrier the stress is mainly relaxed by τ_{arm}. Indeed, as already mentioned, this M_{arm} marks a threshold, beyond which (for longer arms) the terminal relaxation of a GNP is dominated by arm retraction (the dry zone fraction is small enough for the GNPs to diffuse past each other without the barrier, see Figures S13, S14 and Table S5 of the SI).

The hopping potential ΔU_{hop} represents the barrier for cage escape of the GNP with a certain attempt time, and is approximated below by means of a simple scaling analysis, which is based on the compression of a GNP by its neighboring GNPs during its hopping step. Let us consider such a caged GNP in Figure 4 and assume, for simplicity, that it forms three facets during the transition state of the hopping process between neighboring cages. The overall GNP deformation γ_{GNP} is its fractional compression, i.e., $\gamma_{GNP} = 1 - \frac{D}{R}$, where

D represents the size the deformed particle (of initial radius R) as depicted in Figure 4 (estimated values are reported in Table S6 of the SI). The hopping potential is the change in elastic energy of the GNP due to extension of its arms (from initial length h_{pol} to h'_{pol}) because of the creation of the facets (see Figure 4). It is proportional to the change in respective elastic energy per arm, $\frac{{h'_{pol}}^2}{b^2 N_{arm}} - \frac{{h_{pol}}^2}{b^2 N_{arm}}$ (see also Figure S21 of the SI). In addition, we need to account for the number of chains per facet as well as the number of facets (three for the examined GNP and one for each of its three neighbors in the cage, i.e., a total of six facets, see Figure 4). We combined all these coefficients into a single parameter A times the number of arms f and expressed the activated hopping model potential as

$$\Delta U_{hop} = \mathrm{A} f \left(\frac{{h_{pol}}^2}{b^2 N_{arm}} - \frac{{h'_{pol}}^2}{b^2 N_{arm}} \right) k_B T \tag{6}$$

The explicit form of the hopping barrier height is

$$\Delta U_{hop} = A f \left(\frac{R^2 - D^2 + (D - R_{core})^2}{b^2 N_{arm}} - \frac{(R - R_{core})^2}{b^2 N_{arm}} \right) k_B T \tag{7}$$

Using the expression for the GNP radius R (eq. 4) we can estimate the free energy barrier

$$\frac{\Delta U_{hop}}{k_B T} = B \left(\frac{f}{\left(R_{core}^3 / \upsilon_0 \right)^{1/4}} \right)^{4/3} \left(\frac{R_{core}^3}{\upsilon_0 f N_{arm}} \right)^{2/3} \left(1 + \frac{R_{core}^3}{\upsilon_0 f N_{arm}} \right)^{1/3} \tag{8}$$

where the coefficient $B = 2A \left(\frac{3\upsilon_0}{4\pi b^3} \right)^{\frac{2}{3}} \left(1 - \frac{D}{R} \right)$.

Dynamic state diagram.

The condition $\Delta U_{hop} = k_B T$ which marks the transition from polymeric response without barrier to colloidal response, corresponds to

$$\frac{f}{\left(R_{core}^3 / \upsilon_0 \right)^{1/4}} = B^{-3/4} \left(\frac{N_{arm} \upsilon_0 f}{R_{core}^3} \right)^{1/2} \left(1 + \frac{R_{core}^3}{\upsilon_0 f N_{arm}} \right)^{-1/4} \tag{9}$$

Since $\frac{R_{core}^3}{\upsilon_0 f N_{arm}} \ll 1$ in the GNPs and stars (for systems investigated this ratio is ≤0.033), we can simplify the above equation and obtain a simple approximation for the boundary separating Regimes I and II:

$$\frac{f}{\left(R_{core}^3 / \upsilon_0 \right)^{1/4}} = B^{-3/4} \left(\frac{N_{arm} \upsilon_0 f}{R_{core}^3} \right)^{1/2} \tag{10}$$

In Figure 5 we plot experimental data of the normalized number of arms $\frac{f}{\left(R_{core}^3/v_0\right)^{1/4}}$ as a function of the normalized arm size $\frac{N_{arm}v_0 f}{R_{core}^3}$ for various experimental GNPs and stars which have been identified to exhibit polymeric (filled symbols, Regime II) or jammed colloidal (open symbols, Regime I) behaviors, while some (noted by X) exhibit a second weak relaxation mode without a well-discerned low-frequency plateau (extending over at least one decade); it this situation, ΔU_{hop} may slightly exceed k_BT and Z>>1 (in fact, it is $Z_{s,eff}=M_{s,eff}/M_e$ >>1, see Figure 3 and SI). The line separating the polymeric and colloidal responses (Regimes II and I, respectively) is the above eq.10 with a value of the fit parameter B=0.1. This result is very satisfactory and appears to be universal. Details about the investigated multiarm star polybutadienes (1,4-microstructure) with very high branching functionalities (ranging from 875 to 2828, see Table M2), which exhibited colloidal jamming response, are provided in Figures S23–S25, and S27 of the SI.

To justify the values of the parameters A and B, we consider that the average deformation $\gamma_{GNP} = 1 - \frac{D}{R}$ is in the range 0.1 to 0.3. The respective surface of the spherical cap deformed by γ_{GNP} is $2\pi R(R\text{-}D)$ and occupies a fraction of the total GNP surface of $\frac{2\pi R(R-D)}{4\pi R^2} = \frac{\gamma_{GNP}}{2} = 0.05 - 0.15$. The number of chains per facet is $\frac{\gamma_{GNP}}{2} f$. For a total of six facets, this leads to A = $\frac{2\pi R(R-D)}{4\pi R^2} 6 = 3\gamma_{GNP} \approx 0.3 - 0.9$. Note that a number of simplifications/assumptions were used: The degree of interpenetration per arm was considered to be the same, the number of facets was assumed to be 3×2=6, and the deformation per arm was considered to be the same. Since the parameter $\left(\frac{3v_0}{4\pi b^3}\right)^{2/3}$ for different chemistries does not vary substantially (see also SI), we assigned an average value of 0.15 to this parameter. This yields values of B ranging from 0.03 to 0.09, which is close to the value 0.1 selected above. As a consistency check, we compared the potential from eq. 8 with the potential extracted from eqs. 2 and 5 using experimental data for terminal and arm times, and found that the agreement was reasonable (see Figure S22 and Table S7 of the SI).

Using the definition of the overcrowding parameter $x = \frac{f}{\frac{\pi b^2}{v_0}\left(R_{core}^3 + \frac{3fN_{arm}v_0}{4\pi}\right)^{1/3}}$ (see also SI and Ref.33) and eq.9, we can re-write eq.8 as

$$x = \frac{Bf}{\pi\left(\frac{bN_{arm}^{1/2}}{(fv_0)^{1/3}}\right)\left(\frac{bN_{arm}^{1/2}}{R_{core}}\right)} \tag{11}$$

This equation reflects the condition $\Delta U_{hop}=k_BT$, expressed in terms of x, with the right-hand side representing a normalized functionality of the hairy nanoparticle. The inset of Figure 5 plots the same experimental data in terms of this normalized functionality versus x. The data virtually collapse onto a power-law line with exponent of about 7/3. The dashed line is eq.11

with B=0.1 and crosses that data at the point (1,1), which marks the universal transition from colloidal response (Regime I) for $x>1$ to polymeric (Regime II) for $x<1$. Hence, x is the single material parameter to design such systems with desired colloidal vs polymeric response.

Plateau modulus and cage escape.

With the hopping potential being able to describe reasonably the free energy barrier for a GNP to escape from its colloidal cage, as judged from the dynamic diagram of Figure 5, we now use eq.8 to determine the colloidal plateau modulus, which is the hopping barrier per particle volume, $G_{LF}=\frac{\Delta U_{hop}}{R^3}$, and normalize it by the thermal energy per particle volume:

$$\frac{G_{LF}R^3}{k_BT}=CB\left(\frac{f}{\left(R_{core}^3/v_0\right)^{1/4}}\right)^{4/3}\left(\frac{R_{core}^3}{v_0 f N_{arm}}\right)^{2/3}\left(1+\frac{R_{core}^3}{v_0 f N_{arm}}\right)^{1/3} \quad (12)$$

In this equation C is a prefactor which we determine below, while B=0.1 as alredy explained. Reorganization of eq.12 at the transition state where $\Delta U_{hop}=k_BT$ (i.e. by combining with eq. 11) yields

$$\frac{G_{LF}R^3}{k_BT}\approx C \quad (13)$$

We plot in Figure 6 the experimental $\frac{G_{LF}R^3}{k_BT}$ as a function of the overcrowding parameter x. As expected, the normalized modulus is defined only for $x\geq1$ and increases with x. Extrapolation to x=1 yields $\frac{G_{LF}R^3}{k_BT}=5$, which is the above extracted value of C, consistent with eq.13. Using C=5 we can determine the normalized low-frequency modulus from the right-hand side above of eq.12, which is in very good agreement with the experimental data for both GNPs and stars (see Table S8 of the SI).

The terminal time τ_{term}, calculated from eqs. 2, 5 and 8 (using a = 2 and B=0.1) and extracted from the experimental data, is presented in Figure 7 where the different relaxation times are plotted as a function of $Z=N_{arm}/N_e$ (see also Table S7). The agreement of this simple model with the experimental data is quite satisfactory, with a notable deviation for the 130k sample (N_{arm}=263, $Z\approx12$). This is expected, as the potential is larger in the jammed regime with large differences between the terminal and arm relaxation times (and large ΔU_{hop}), whereas in the polymeric high-Z regime there is no attempt process (see Figure 3 and Figures S15–S20 of the SI) and the MM model works satisfactorily. The terminal relaxation time is nearly constant for $Z<10$ (while the arm relaxation time increases), and much larger than the arm relaxation time (up to 5 decades), while it decreases for larger Z values, eventually approaching the arm relaxation time. The open red and blue circles in Figure 7 represent the τ_{arm} estimated from the MM best fit to the experimental data (as outlined above) and the MM model prediction based on the relaxation

of arm segments with a degree of polymerization N_{inter} calculated with the two-layer model, respectively (see Figures S15–S20 of the SI). The deviations suggest there are still subtle details in both the two-layer model and the MM analysis of arm relaxation in densely grafted nanoparticles and require further consideration in the future. However, they do not affect the emerging clear picture of transition from polymeric to colloidal dynamics at x=1 (at about Z≈12 for the present GNPs) as presented in Figure 5. Note that N_{inter} and N_{seff} deviate as Z increases (see Figure S13), and the associated arm relaxation times extracted from the two-layer and MM models differ. We attribute this, in part, to the approximate formulation of the partial arm retraction model in eq.1, as well as the fact that the two-layer model is essentially applicable for x≥1 (since for x<<1 it considers that arms overlap only with nearest neighbors), but more work will be needed to properly address this point. Another important point is the fact that a sizeable core would induce a steric repulsive constraint (retardation) on the arm retraction process, which is not accounted for here.[77,78] The ratio $R_c / <R^2>^{1/2}$ is small in the studied experimental nanoparticles (it varies from 0.27 to 0.48 for GNPs and 0.29 to 0.44 for stars) but not negligible, hence its role on arm retraction should also be addressed in the future (along with possible chain stretching near the core). In this context, we recall that the largest discrepancies in the values of N_{inter} extracted from the MM fit were observed for the largest values of $R_c / <R^2>^{1/2}$. We emphasize that these considerations could lead to improvements in the quantitative description of the dynamics, which however do not influence the message of the present work. Also depicted in Figure 7 are the predicted τ_{term} (open inverted triangles), from eq.2, and attempt $\tau_{attempt}$ (asterisks), from eq.5, times which are discussed below in the context of the slow mode analysis. The remarkable structural change experienced by the GNPs with increasing N_{arm} is also reflected in the dependence of their zero-shear rate viscosity on M_{arm} (see Figure S11 of the SI).

CONCLUSIONS

We have shown how to decouple the dynamics of self-suspended hairy particles (grafted nanoparticles and star polymers in the melt state) into polymeric and colloidal contributions, and at the same time, their dynamics can be tailored from polymeric (viscoelastic liquid) to jammed colloidal, by varying the size of the grafted chain at fixed grafting density and core size. The former can be described quantitatively by a tube-based arm relaxation model and the latter by invoking a simple hopping model based on the elastic deformation of the caged particles. A transition from polymeric to jammed colloidal response is observed when the hopping potential becomes ~k_BT. which is shown to correspond to a value of the overcrowding parameter x=1. Hence, this structural parameter is now linked to the energetic barrier for hopping. Further, this allows constructing a universal dynamic state diagram in terms of normalized number of arms $\frac{f}{\left(R_{core}^3/\upsilon_0\right)^{1/4}}$ as a function of their normalized size $\frac{N_{arm}\upsilon_0 f}{R_{core}^3}$, applicable to a wide range of self-suspended hairy nanoparticles. Despite its simplicity our approach is robust and represents a first-order guide for the cross-over between colloidal and polymeric regimes in this class of materials, which is controlled by a single materials property, the overlapping parameter x. There are still many open questions such as how variations in chain extension in the dry zone can modify the arm retraction

model, or how to make the hopping potential model more realistic by better estimating the number of facets, the number of arms in the interpenetration zone and the degree of interpenetration per arm.

Experimental Details

Materials and Methods

Grafted nanoparticles: Poly(methylacrylate) (PMA)-grafted silica (SiO_2) nanoparticles (16±4 nm core diameter, 0.47±0.4 chains/nm^2 grafting density) were synthesized by the surface-initiated reversible addition-fragmentation chain transfer polymerization (SI-RAFT) technique.[1,79] Details on the synthetic process and the reaction mechanisms can be found elsewhere.[80] The molecular characteristics of the investigated systems are reported in Table M1. The entanglement molar mass of PMA is 11 kg/mol. Details on differential scanning calorimetry measurements and thermal gravimetric analysis (TGA) are described in Ref. 80. Small angle X-ray scattering results are shown in Figure S26 of the SI. The samples were all studied in the molten state. To mold the samples, approximately 65–75 mg of material was loaded into an 8 mm diameter stainless steel vacuum mold to yield disks of approximately 800–1000 μm thickness. Vacuum was applied inside the mold by connecting a hose on the chamber to the inlet of an air compressor. The mold was heated to 80 °C for 20 minutes and then allowed to cool gradually to room temperature, while maintained under vacuum. Depending on the experiment, 4 mm and 2 mm disks were also used.

Multiarm star polymers: Polybutadiene (1,4 microstructure) stars, synthesized and characterized as described by Gauthier and Munam,[81] were used for additional data (see Table M2 for the molecular characteristics). The new stars used here have the following characteristics (based on chemical characterization)[81]: $f = 1114$, $M_{arm} = 1270$ g/mol and $f = 2828$, $M_{arm} = 1300$ g/mol, with polydispersity below 1.1, see Table M2. Small angle X-ray scattering results for some stars are reported in Figure S27 of the SI. Specimens for rheological tests were press-molded under vacuum into 4 mm disks.

Small Amplitude Oscillatory Shear and Creep measurements: Oscillatory shear experiments were conducted on an ARES stress-controlled rheometer using either an 8, 4 or 2 mm parallel plate geometry. The temperature was controlled by a convection oven fed with nitrogen gas to minimize sample degradation. Creep experiments were performed on an Anton Paar MCR702 instrument equipped with 8 mm parallel plates. After loading, typically at 80 °C, the samples were allowed to equilibrate for at least 30 minutes. Strain sweep experiments were carried out to determine their linear viscoelastic regime at each temperature. Dynamic time sweep experiments in the linear regime were also performed to ensure steady-state and thermal equilibrium conditions. Frequency sweeps were conducted from 100 – 0.1 rad/s at 5 °C intervals from 80 °C to 30 °C and at 2–3°C intervals between 27°C to 18°C (the latter corresponds to the glass transition temperature). Small amplitude oscillatory shear experiments for stars were performed in an ARES stress-controlled rheometer using a 4 mm parallel plate geometry in the temperature range −80 to 30 °C. The temperature was controlled with a convection oven connected to a liquid nitrogen Dewar container.

Supplementary Material

Refer to Web version on PubMed Central for supplementary material.

Acknowledgments

Partial support by the EU (ETN-COLLDENSE, H2020-MCSA-ITN-2014, Grant No. 642774) and the Greek Secretariat for Research and Technology (INNOVATION program-AENAO) is gratefully acknowledged. MR acknowledges financial support from National Science Foundation under Grant EFMA-1830957 and the National Institutes of Health under Grant P01-HL108808. SK acknowledges financial support for this research from the Department of Energy under grant DE-SC0021272. We thank Mayank Jhalaria for help in sample preparation and for many deep discussions on the topic of this paper.

References

(1). Li C; Han J; Ryu CY; Benicewicz BC A Versatile Method to Prepare RAFT Agent Anchored Substrates and the Preparation of PMMA Grafted Nanoparticles. Macromolecules 2006, 39 (9), 3175–3183.

(2). Chevigny C; Dalmas F; Di Cola E; Gigmes D; Bertin D; Boué F; Jestin J. Polymer-Grafted-Nanoparticles Nanocomposites: Dispersion, Grafted Chain Conformation, and Rheological Behavior. Macromolecules 2010, 44 (1), 122–133.

(3). Kumar SK; Jouault N; Benicewicz B; Neely T. Nanocomposites with Polymer Grafted Nanoparticles. Macromolecules 2013, 46 (9), 3199–3214.

(4). Mangal R; Srivastava S; Archer LA Phase Stability and Dynamics of Entangled Polymer–Nanoparticle Composites. Nature Communications 2015, 6, 7198.

(5). Alkhodairi H; Russell ST; Pribyl J; Benicewicz BC; Kumar SK Compatibilizing Immiscible Polymer Blends with Sparsely Grafted Nanoparticles. Macromolecules 2020, 53 (23), 10330–10338.

(6). Hore MJ Polymers on Nanoparticles: Structure & Dynamics. Soft Matter 2019, 15 (6), 1120–1134. [PubMed: 30657158]

(7). Meng D; Kumar SK; Lane JMD; Grest GS Effective Interactions between Grafted Nanoparticles in a Polymer Matrix. Soft Matter 2012, 8 (18), 5002–5010.

(8). Chremos A; Panagiotopoulos AZ; Koch DL Dynamics of Solvent-Free Grafted Nanoparticles. The Journal of Chemical Physics 2012, 136 (4), 044902.

(9). Sunday D; Ilavsky J; Green DL A Phase Diagram for Polymer-Grafted Nanoparticles in Homopolymer Matrices. Macromolecules 2012, 45 (9), 4007–4011.

(10). Moll JF; Akcora P; Rungta A; Gong S; Colby RH; Benicewicz BC; Kumar SK Mechanical Reinforcement in Polymer Melts Filled with Polymer Grafted Nanoparticles. Macromolecules 2011, 44 (18), 7473–7477.

(11). Srivastava S; Agarwal P; Archer LA Tethered Nanoparticle–Polymer Composites: Phase Stability and Curvature. Langmuir 2012, 28 (15), 6276–6281. [PubMed: 22439646]

(12). Lin C-C; Griffin PJ; Chao H; Hore MJ; Ohno K; Clarke N; Riggleman RA; Winey KI; Composto RJ Grafted Polymer Chains Suppress Nanoparticle Diffusion in Athermal Polymer Melts. The Journal of Chemical Physics 2017, 146 (20), 203332. [PubMed: 28571331]

(13). Pakula T. Static and Dynamic Properties of Computer Simulated Melts of Multiarm Polymer Stars. Computational and Theoretical Polymer Science 1998, 8 (1–2), 21–30.

(14). Chremos A; Panagiotopoulos AZ Structural Transitions of Solvent-Free Oligomer-Grafted Nanoparticles. Physical Review Letters 2011, 107 (10), 105503.

(15). Bilchak CR; Buenning E; Asai M; Zhang K; Durning CJ; Kumar SK; Huang Y; Benicewicz BC; Gidley DW; Cheng S. Polymer-Grafted Nanoparticle Membranes with Controllable Free Volume. Macromolecules 2017, 50 (18), 7111–7120.

(16). Agarwal P; Qi H; Archer LA The Ages in a Self-Suspended Nanoparticle Liquid. Nano letters 2009, 10 (1), 111–115.

(17). Choudhury S; Agrawal A; Kim SA; Archer LA Self-Suspended Suspensions of Covalently Grafted Hairy Nanoparticles. Langmuir 2015, 31 (10), 3222–3231. [PubMed: 25712578]

(18). Srivastava S; Choudhury S; Agrawal A; Archer LA Self-Suspended Polymer Grafted Nanoparticles. Current Opinion in Chemical Engineering 2017, 16, 92–101.

(19). Choi J; Hore MJ; Clarke N; Winey KI; Composto RJ Nanoparticle Brush Architecture Controls Polymer Diffusion in Nanocomposites. Macromolecules 2014, 47 (7), 2404–2410.

(20). Sakib N; Koh YP; Huang Y; Mongcopa KIS; Le AN; Benicewicz BC; Krishnamoorti R; Simon SL Thermal and Rheological Analysis of Polystyrene-Grafted Silica Nanocomposites. Macromolecules 2020, 53 (6), 2123–2135.

(21). Gohr K; Pakula T; Tsutsumi K; Schärtl W. Dynamics of Copolymer Micelles in an Entangled Homopolymer Matrix. Macromolecules 1999, 32 (21), 7156–7165.

(22). Hasegawa R; Aoki Y; Doi M. Optimum Graft Density for Dispersing Particles in Polymer Melts. Macromolecules 1996, 29 (20), 6656–6662.

(23). Liu X; Utomo NW; Zhao Q; Zheng J; Zhang D; Archer LA Effects of Geometric Confinement on Caging and Dynamics of Polymer-Tethered Nanoparticle Suspensions. Macromolecules 2021, 54 (1), 426–439.

(24). Watanabe H. Rheology of diblock copolymer micellar systems. Acta polymerica 48.7 1997: 215–233.

(25). Sebastian JM, Lai C, Graessley WW, Register RA, and Marchand GR (2002). Steady-shear rheology of block copolymer melts: Zero-shear viscosity and shear disordering in body-centered-cubic systems. Macromolecules 2002, 35(7), 2700–2706.

(26). Sebastian John M., Graessley William W., and Register Richard A. “Steady-shear rheology of block copolymer melts and concentrated solutions: Defect-mediated flow at low stresses in body-centered-cubic systems.” Journal of Rheology 46.4 2002: 863–879.

(27). Daoud M, and Cotton JP “Star shaped polymers: a model for the conformation and its concentration dependence.” Journal de Physique 43.3 1982: 531–538.

(28). Pham QT, Russel WB, Thibeault JC, and Lau W. Micellar solutions of associative triblock copolymers: Entropic attraction and gas− liquid transition. Macromolecules, 32(9) 1999, 2996–3005.

(29). Liu X; Abel BA; Zhao Q; Li S; Choudhury S; Zheng J; Archer LA Microscopic Origins of Caging and Equilibration of Self-Suspended Hairy Nanoparticles. Macromolecules 2019, 52 (21), 8187–8196.

(30). Pakula T; Vlassopoulos D; Fytas G; Roovers J. Structure and Dynamics of Melts of Multiarm Polymer Stars. Macromolecules 1998, 31 (25), 8931–8940.

(31). Vlassopoulos D. Macromolecular Topology and Rheology: Beyond the Tube Model. Rheologica Acta 2016, 55 (8), 613–632.

(32). Vlassopoulos D; Cloitre M. Tunable Rheology of Dense Soft Deformable Colloids. Current Opinion in Colloid & Interface Science 2014, 19 (6), 561–574.

(33). Kapnistos M; Semenov AN; Vlassopoulos D; Roovers J. Viscoelastic Response of Hyperstar Polymers in the Linear Regime. The Journal of Chemical Physics 1999, 111 (4), 1753–1759.

(34). Gury L; Gauthier M; Cloitre M; Vlassopoulos D. Colloidal Jamming in Multiarm Star Polymer Melts. Macromolecules 2019, 52 (12), 4617–4623.

(35). Ferreira PG; Ajdari A; Leibler L. Scaling Law for Entropic Effects at Interfaces between Grafted Layers and Polymer Melts. Macromolecules 1998, 31 (12), 3994–4003.

(36). Leibler L; Ajdari A; Mourran A; Coulon G; Chatenay D. Proceedings of the Ordering in Macromolecular Systems, OUMS Conference, Osaka, Japan,(1993). 1994.

(37). Raphael E; Pincus P; Fredrickson GH Conformation of Star Polymers in High-Molecular-Weight Solvents. Macromolecules 1993, 26 (8), 1996–2006.

(38). Midya J; Rubinstein M; Kumar SK; Nikoubashman A. Structure of Polymer-Grafted Nanoparticle Melts. ACS nano 2020, 14 (11), 15505–15516. [PubMed: 33084300]

(39). Halim A; Fu Q; Yong Q; Gurr PA; Kentish SE; Qiao GG Soft Polymeric Nanoparticle Additives for next Generation Gas Separation Membranes. Journal of Materials Chemistry A 2014, 2 (14), 4999–5009.

(40). Ahn SH; Park JT; Kim JH; Ko Y; Hong SU Nanocomposite Membranes Consisting of Poly (Vinyl Chloride) Graft Copolymer and Surface-Modified Silica Nanoparticles. Macromolecular research 2011, 19 (11), 1195.

(41). Kwon Y; Im H; Kim J. Effect of PMMA-Graft-Silica Nanoparticles on the Gas Permeation Properties of Hexafluoroisopropylidene-Based Polyimide Membranes. Separation and purification technology 2011, 78 (3), 281–289.

(42). Ghosal K; Freeman BD Gas Separation Using Polymer Membranes: An Overview. Polymers for advanced technologies 1994, 5 (11), 673–697.

(43). Bilchak CR; Jhalaria M; Huang Y; Abbas Z; Midya J; Benedetti FM; Parisi D; Egger W; Dickmann M; Minelli M. Tuning Selectivities in Gas Separation Membranes Based on Polymer-Grafted Nanoparticles. ACS nano 2020. 14 (12), 17174–17183.

(44). Ramesh N; Davis PK; Zielinski JM; Danner RP; Duda JL Application of Free-Volume Theory to Self Diffusion of Solvents in Polymers below the Glass Transition Temperature: A Review. Journal of Polymer Science Part B: Polymer Physics 2011, 49 (23), 1629–1644.

(45). Popov I; Carroll B; Bocharova V; Genix A-C; Cheng S; Khamzin A; Kisliuk A; Sokolov AP Strong Reduction in Amplitude of the Interfacial Segmental Dynamics in Polymer Nanocomposites. Macromolecules 2020, 53 (10), 4126–4135.

(46). Ge S; Samanta S; Tress M; Li B; Xing K; Dieudonné-George P; Genix A-C; Cao P-F; Dadmun M; Sokolov AP Critical Role of the Interfacial Layer in Associating Polymers with Microphase Separation. Macromolecules 2021, 54 (9), 4246–4256.

(47). Kardasis P; Kalafatakis N; Gauthier M; Vlassopoulos D; Floudas G. Layers of Distinct Mobility in Densely Grafted Dendrimer Arborescent Polymer Hybrids. Physical Review Letters 2021, 126 (20), 207802.

(48). Fetters LJ; Lohse DJ; Colby RH Chain Dimensions and Entanglement Spacings. In Physical properties of polymers handbook; Springer, 2007; pp 447–454.

(49). Guth E. Theory of Filler Reinforcement. Journal of applied physics 1945, 16 (1), 20–25.

(50). Wolff S; Donnet J-B Characterization of Fillers in Vulcanizates According to the Einstein-Guth-Gold Equation. Rubber chemistry and technology 1990, 63 (1), 32–45.

(51). Rubinstein M; Colby RH Polymer Physics; Oxford University Press New York, 2003.

(52). Snijkers F; Ratkanthwar K; Vlassopoulos D; Hadjichristidis N. Viscoelasticity, Nonlinear Shear Start-up, and Relaxation of Entangled Star Polymers. Macromolecules 2013, 46 (14), 5702–5713.

(53). Erwin BM; Cloitre M; Gauthier M; Vlassopoulos D. Dynamics and Rheology of Colloidal Star Polymers. Soft Matter 2010, 6 (12), 2825.

(54). Parisi D; Ruiz-Franco J; Ruan Y; Liu CY; Loppinet B; Zaccarelli E; Vlassopoulos D. Static and Dynamic Properties of Block Copolymer Based Grafted Nanoparticles across the Non-Ergodicity Transition. Physics of Fluids 2020, 32 (12), 127101.

(55). Pusey PN; Segre PN; Behrend OP; Meeker SP; Poon WCK Dynamics of Concentrated Colloidal Suspensions. Physica A: Statistical Mechanics and its Applications 1997, 235 (1–2), 1–8.

(56). Zaccarelli E; Poon WC Colloidal Glasses and Gels: The Interplay of Bonding and Caging. Proceedings of the National Academy of Sciences 2009, 106 (36), 15203–15208.

(57). Weese J. A Regularization Method for Nonlinear Ill-Posed Problems. Computer Physics Communications 1993, 77 (3), 429–440.

(58). Elster C; Honerkamp J; Weese J. Using Regularization Methods for the Determination of Relaxation and Retardation Spectra of Polymeric Liquids. Rheologica Acta 1992, 31 (2), 161–174.

(59). Honerkamp J; Weese J. A Nonlinear Regularization Method for the Calculation of Relaxation Spectra. Rheologica acta 1993, 32 (1), 65–73.

(60). Ferry JD Viscoelastic Properties of Polymers; John Wiley & Sons, 1980.

(61). Bacová P; Lentzakis H; Read DJ; Moreno AJ; Vlassopoulos D; Das C. Branch-Point Motion in Architecturally Complex Polymers: Estimation of Hopping Parameters from Computer Simulations and Experiments. Macromolecules 2014, 47 (10), 3362–3377.

(62). Williams ML; Landel RF; Ferry JD The Temperature Dependence of Relaxation Mechanisms in Amorphous Polymers and Other Glass-Forming Liquids. Journal of the American Chemical society 1955, 77 (14), 3701–3707.

(63). Walsh D; Zoller P. Standard Pressure Volume Temperature Data for Polymers; CRC Press, 1995.

(64). Kuzuu N; Nagai K; Tanaka M; Tamai Y. Molecular Dynamics Study of Fictive Temperature Dependence of Density of Vitreous Silica. Japanese journal of applied physics 2005, 44 (10R), 7550.

(65). Milner ST; McLeish TCB Parameter-Free Theory for Stress Relaxation in Star Polymer Melts. Macromolecules 1997, 30 (7), 2159–2166.

(66). Milner ST; McLeish TCB Reptation and Contour-Length Fluctuations in Melts of Linear Polymers. Physical Review Letters 1998, 81 (3), 725.

(67). Likhtman AE; McLeish TC Quantitative Theory for Linear Dynamics of Linear Entangled Polymers. Macromolecules 2002, 35 (16), 6332–6343.

(68). Colby RH; Rubinstein M. Two-Parameter Scaling for Polymers in θ Solvents. Macromolecules 1990, 23 (10), 2753–2757.

(69). Rubinstein M; Obukhov SP Power-Law-like Stress Relaxation of Block Copolymers: Disentanglement Regimes. Macromolecules 1993, 26 (7), 1740–1750.

(70). Cai L-H; Panyukov S; Rubinstein M. Hopping Diffusion of Nanoparticles in Polymer Matrices. Macromolecules 2015, 48 (3), 847–862. [PubMed: 25691803]

(71). Semenov AN Rheology of Polymer Brushes: Rouse Model. Langmuir 1995, 11 (9), 3560–3564.

(72). Witten TA; Leibler L; Pincus PA Stress Relaxation in the Lamellar Copolymer Mesophase. Macromolecules 1990, 23 (3), 824–829.

(73). Vlassopoulos D; Fytas G; Pakula T; Roovers J. Multiarm Star Polymers Dynamics. Journal of Physics: Condensed Matter 2001, 13 (41), R855.

(74). Fetters LJ; Kiss AD; Pearson DS; Quack GF; Vitus FJ Rheological Behavior of Star-Shaped Polymers. Macromolecules 1993, 26 (4), 647–654.

(75). Johnson KJ; Glynos E; Sakellariou G; Green P. Dynamics of Star-Shaped Polystyrene Molecules: From Arm Retraction to Cooperativity. Macromolecules 2016, 49 (15), 5669–5676.

(76). Pakula T, Geyler S, Edling T, and Boese D. Relaxation and viscoelastic properties of complex polymer systems. Rheologica Acta 1996, 35(6), 631–644.

(77). Sato T, Watanabe H, Osaki K, and Yao ML Relaxation of spherical micellar systems of styrene−isoprene diblock copolymers. 1. Linear viscoelastic and dielectric behavior. Macromolecules, 29(11) 1996, 3881–3889.

(78). Watanabe H. Rheology of diblock copolymer micellar systems. Acta polymerica 48.7 1997: 215–233.

(79). Barbey R; Lavanant L; Paripovic D; Schuwer N; Sugnaux C; Tugulu S; Klok H-A Polymer Brushes via Surface-Initiated Controlled Radical Polymerization: Synthesis, Characterization, Properties, and Applications. Chemical reviews 2009, 109 (11), 5437–5527. [PubMed: 19845393]

(80). Buenning E. Ph.D. Thesis. Controllable Free-Volume in Polymer-Grafted Nanoparticle Membranes: Origins, Characterization, and Applications. Columbia University, New York, 2018.

(81). Gauthier M; Munam A. Synthesis of 1, 4-Polybutadiene Dendrimer- Arborescent Polymer Hybrids. Macromolecules 2010, 43 (8), 3672–3681.

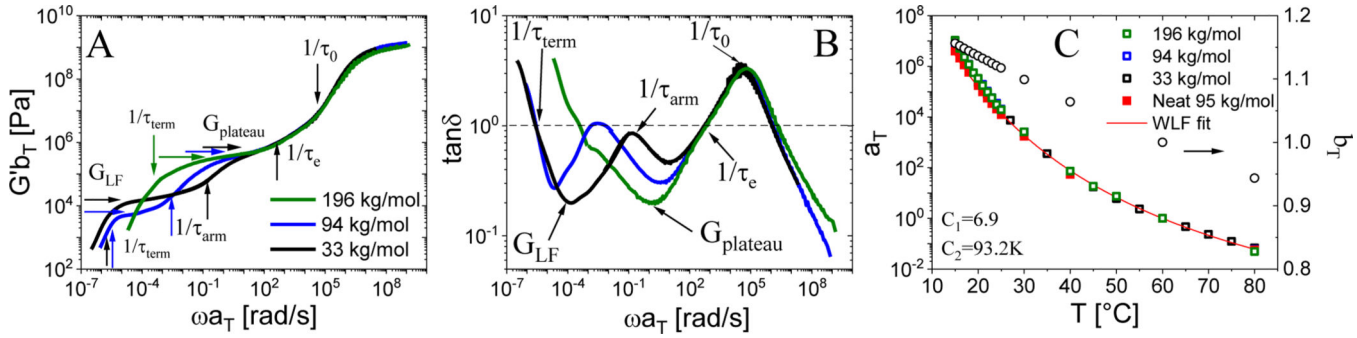

Figure 1.

Linear viscoelastic master curves in terms of A) shifted storage modulus ($G'b_T$) and B) loss factor ($\tan\delta$) at the same relative temperature above T_g (T-T_g = 40 °C) as a function of the shifted oscillatory frequency (ωa_T). Panel C shows the corresponding horizontal (squares) and vertical (circles) shift factors. Black arrows in panels A and B mark the characteristic times (as inverse frequencies) and plateau moduli for the systems (see text), and the horizontal dashed line in panel B refers to equal storage and loss moduli ($G' = G''$, $\tan\delta = 1$). The red solid line in panel C represents the Williams-Landel-Ferry (WLF) fit whose constants are also reported in the graph for T_{ref} = 60 °C. The shift factors for neat PMA 95k are also reported as solid red squares.

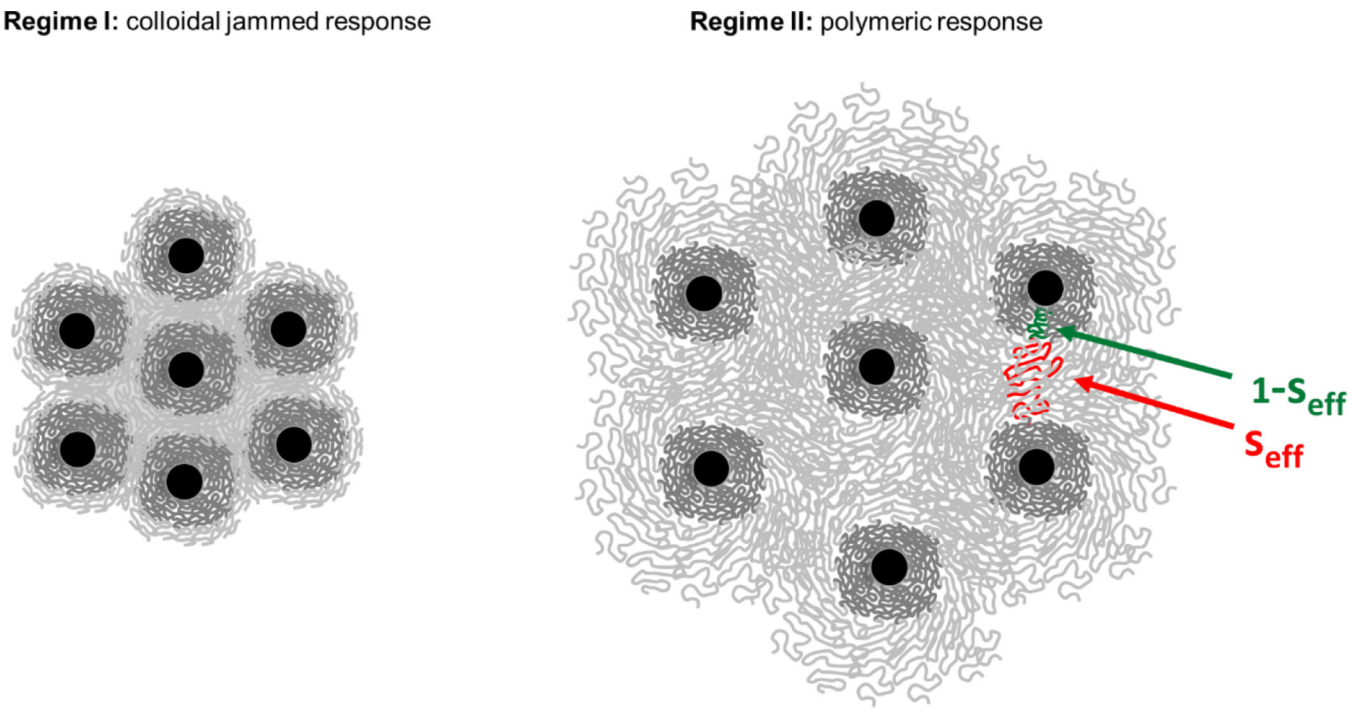

Figure 2.

Schematic representation of GNP melts. Each GNP comprises a nanoparticle core (black), dry and wet layers (impenetrable to and interpenetrated by the arms of neighboring GNPs, respectively), the size of which depends on the grafting density (which is constant here) and the degree of polymerization of the grafted chains. The purposely marked dense (dark) near-core region represents the dry layer (green portion of the colored arm in Regime II), while the interstitial area is the interpenetrated (or wet) layer region (red portion of the arm in Regime II). These two regions correspond to arm fractions (1-s_{eff}) and s_{eff}, respectively, in eq. 1 (see text). In Regime I, the terminal relaxation (if attainable) is dominated by a colloidal-jammed response, and in Regime II by polymeric arm relaxation. The crossover from Regime I to Regime II is broad (see text).

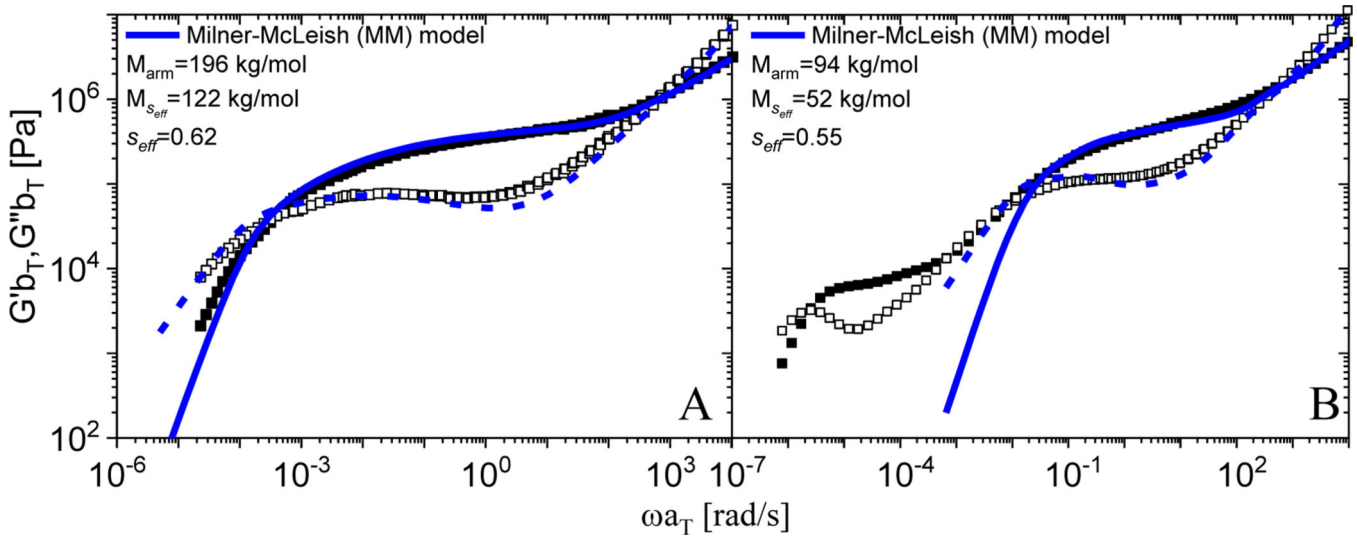

Figure 3.

Linear viscoelastic master curves in terms of shifted storage ($G'b_T$) and loss ($G''b_T$) moduli as a function of the shifted oscillatory frequency (ωa_T) at 40 °C above the glass transition temperature (T-T_g = 40 °C) for the GNP samples 196k (Panel A) and 94k (Panel B). The solid and dashed blue lines represent the storage and loss moduli obtained from the MM model, respectively. M_{arm} is the total arm molar mass, s_{eff} is the fraction of the arm in the interpenetration layer, corresponding to a molar mass M_{seff}.

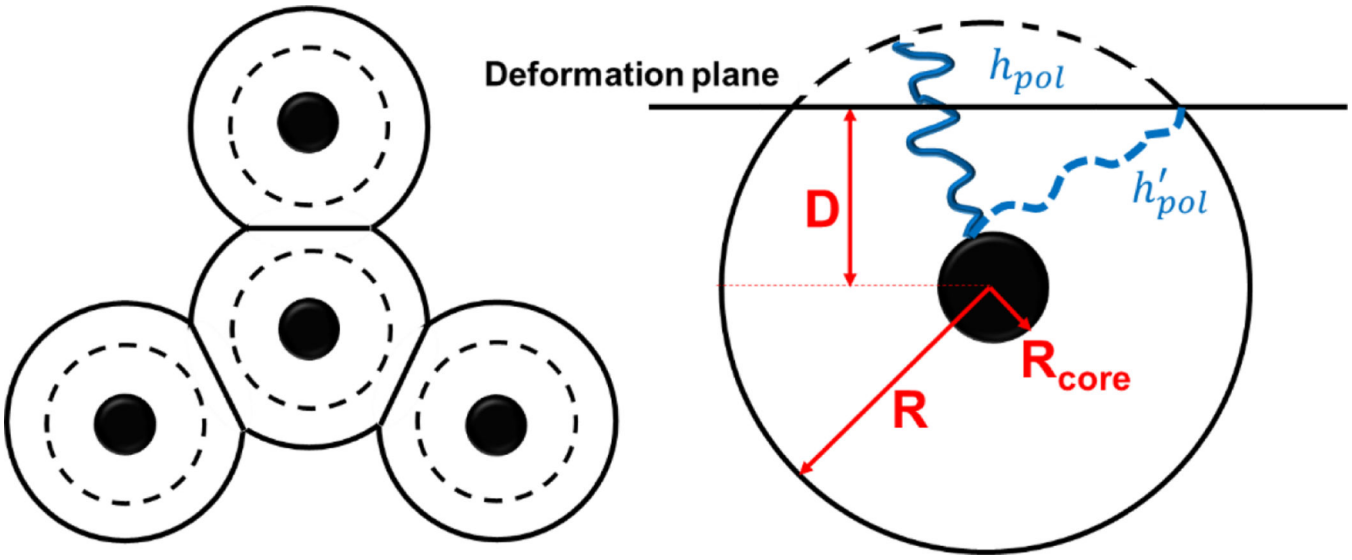

Figure 4.

Schematic representation of deformed particles forming facets (left side), and arm stretching events during particle deformation (right side). D is the depth of the deformation plane, and h_{pol} and h'_{pol} are, respectively, the length of the chains prior to and after deformation sets in.

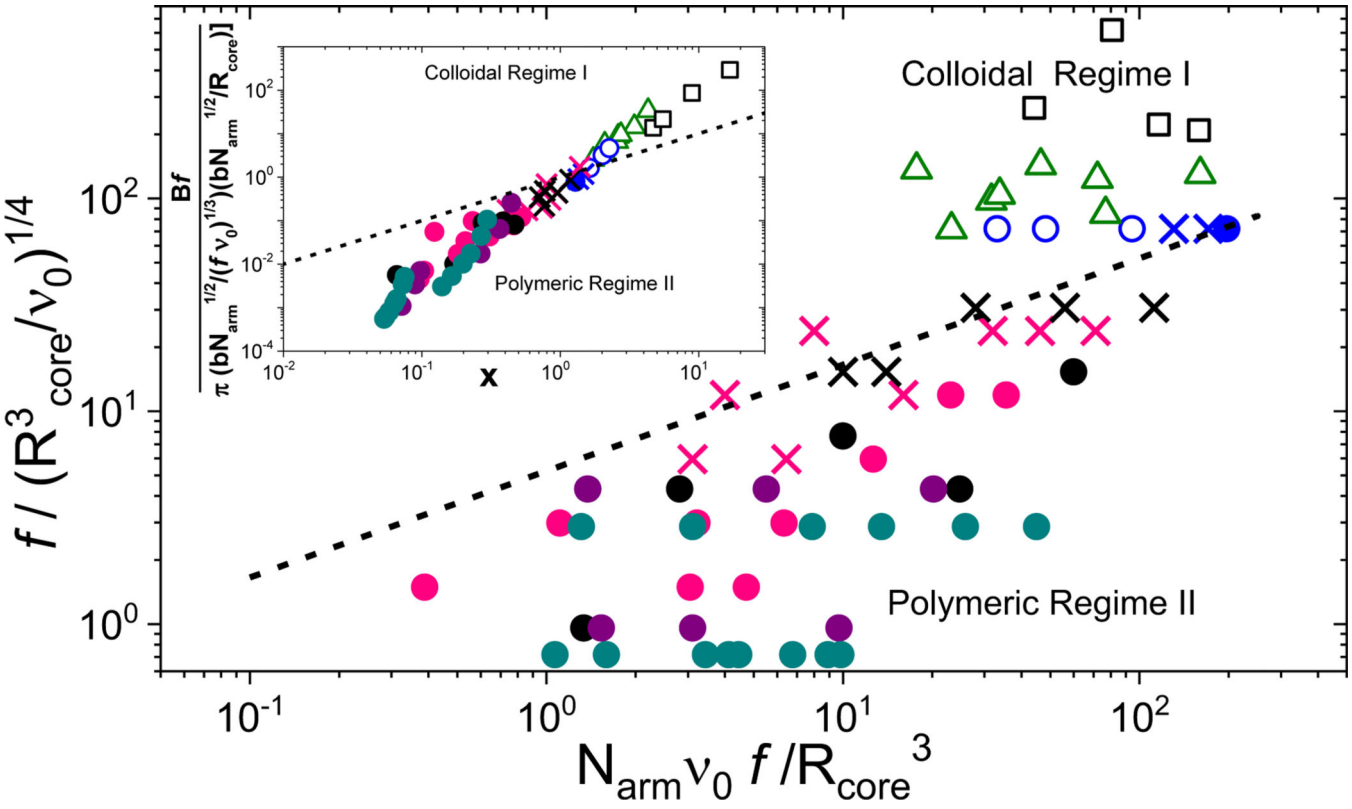

Figure 5.

Dynamic state diagram for GNPs and stars in terms of $\frac{f}{\left(R^3_{core}/\upsilon_0\right)^{1/4}}$ against $\frac{N_{arm}\upsilon_0 f}{R^3_{core}}$ (see text). The filled circles represent systems whose dynamics are controlled by polymeric arm relaxation, cross symbols (X) refer to systems exhibiting hybrid (both polymeric and colloidal) response; in this case, the potential barrier for hopping exceeds k_BT and $Z_{s,eff}$>>1, and open symbols refer to the jammed colloidal regime where an extended low-frequency colloidal mode (with a long relaxation time, if reached, as compared with the arm time) dominates the rheological spectrum. The blue symbols represent the present GNPs. The open green triangles are PEO GNPs from Refs.16,29, and black squares refer to star polymers investigated here (Figures S23–S25) and partially in Ref. 34. The black crosses and circles are star polymers from the literature.[30,33,73] Polyisoprene (PI) stars with low functionalities f = 3 and f = 12, and f = 4 and f = 18, taken from the literature, are displayed as filled dark cyan[74] and filled purple circles,[75] respectively. Polystyrene stars with a branching functionality in the range 2–64, taken from the literature,[76] are displayed as magenta filled circles and crosses. Dashed line is eq. 10 and dotted line is eq.9. Inset: Alternative double logarithmic representation of the main plot with the experimental data being plotted as the normalized functionality of the hairy nanoparticles versus overlap parameter x. The dashed line is eq.11 with B=0.1.

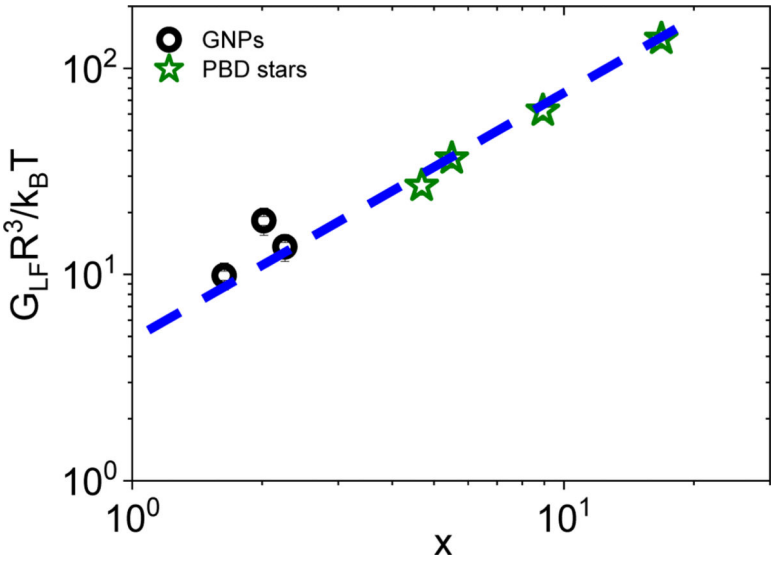

Figure 6.

Experimental normalized low-frequency colloidal plateau modulus as a function of the overcrowding parameter for the GNPs and star PBDs investigated here. The blue dashed line through the data hits the ordinate at a value $\frac{G_{LF}R^3}{k_BT} = 5$.

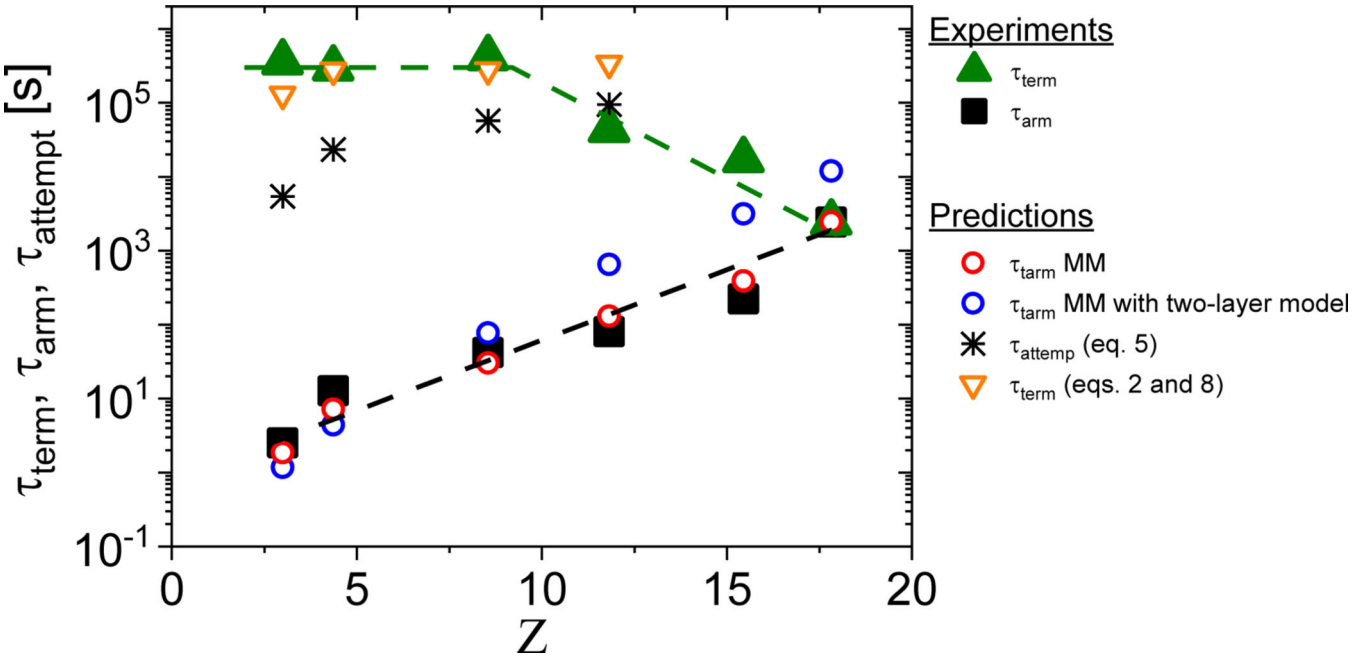

Figure 7.

Experimental terminal (green filled up triangles) and arm relaxation (black filled squares) times for the GNPs, obtained from tanδ (Figure 1), as a function of Z, the number of entanglements per grafted arm. The circles, open down triangles and asterisks represent the model predictions for the arm, attempt and terminal relaxation times (see text), respectively. The dashed lines are drawn through experimental points to guide the eye.

Table M1.

Molecular characteristics of silica-grafted nanoparticles.

Sample code	$M_{w,arm}$ [kg/mol]	Polydispersity of arms	ϕ_{core} (SiO_2 only)	ϕ_{core} (SAXS)	ϕ_{core} (TGA)	T_g [°C]
196k	196	1.3	0.021		unavailable	
170k	170	1.29	0.024	0.036	0.031	18.1
130k	130	1.28	0.031	0.051	0.043	unavailable
94k	94	1.2	0.043	0.07	unavailable	18
48k	48	1.16	0.081	0.139	0.12	18.1
33k	33	1.14	0.112	0.176	0.16	18.3

Author Manuscript

Author Manuscript

Author Manuscript

Table M2.

Molecular characteristics of multi-arm star polymers.

f	M_{arm} [kg/mol]	Polydispersity linear chains
875	5.8	1.08
929	4.0	1.03
1114	1.27	1.07
2828	1.3	1.10